Article citation info:
KANG R, WANG J, CHENG J, CHEN J, PANG Y. Intelligent forecasting of automatic train protection system failure rate in China high-speed railway. Eksploatacja i Niezawodnosc – Maintenance and Reliability 2019; 21 (4): 567–576, http://dx.doi.org/10.17531/ein.2019.4.5.

Renwei KANG
Junfeng WANG
Jianfeng CHENG
Jianqiu CHEN
Yanzhi PANG

INTELLIGENT FORECASTING OF AUTOMATIC TRAIN PROTECTION SYSTEM FAILURE RATE IN CHINA HIGH-SPEED RAILWAY

INTELIGENTNE PROGNOZOWANIE INTENSYWNOŚCI USZKODZEŃ AUTOMATYCZNEGO SYSTEMU OCHRONY POCIĄGÓW KOLEI DUŻYCH PRĘDKOŚCI W CHINACH

Intelligent and personalized dynamic maintenance and spare parts configuration of high-speed railway have been the main trend to guarantee the safety capability of trains. In this paper, a new Automatic Train Protection (ATP) system failure rate calculation method is proposed, and the delay time and embedded dimension are determined by C-C algorithm. Then the phase space is reconstructed from one-dimensional time series to high-dimensional space. Based on chaotic characteristics of failure rate, a short-term intelligent forecasting model of failure rate of ATP system is established. The actual failure statistics from 2010 to 2018 are used as samples to train and test the validity of the model. From prediction results, it shows that the proposed chaos prediction model has an accuracy of 99.71%, which is better than the support vector machine model. Through the intelligent prediction of failure rate, this paper solves the maintenance inflexibility and imbalance of supply and demand of spare parts configuration.

Keywords: *intelligent maintenance, high-speed railway, failure rate, automatic train protection system, prediction model, chaos.*

Inteligentna i spersonalizowana dynamiczna konserwacja i konfiguracja części zamiennych pociągów kolei dużych prędkości stanowią ostatnio główny trend w zakresie zapewniania bezpieczeństwa pociągów. W niniejszym artykule zaproponowano nową metodę obliczania intensywności uszkodzeń systemu Automatycznej Ochrony Pociągu (ATP), a czas opóźnienia i wymiar zanurzenia określano za pomocą algorytmu CC. Następnie, przestrzeń fazową przekształcono z jednowymiarowego szeregu czasowego do przestrzeni wielowymiarowej. Opierając się na chaotycznych charakterystykach intensywności uszkodzeń, utworzono model krótkoterminowego inteligentnego prognozowania awaryjności systemu ATP. Do uczenia modelu i weryfikacji jego trafności wykorzystano rzeczywiste dane statystyczne dotyczące awarii pociągów z lat 2010–2018. Z wyników prognoz wynika, że proponowany model predykcji, oparty na teorii chaosu, cechuje się dokładnością na poziomie 99,71%, czyli wyższą niż model maszyny wektorów nośnych. Dając możliwość inteligentnej predykcji intensywności uszkodzeń, niniejsza praca rozwiązuje problem braku elastyczności w utrzymaniu ruchu pociągów oraz braku równowagi między podażą a popytem na części zamienne.

Słowa kluczowe: *inteligentna konserwacja, kolej dużych prędkości, intensywność uszkodzeń, automatyczny system ochrony pociągu, model predykcyjny, chaos.*

1. Introduction

China high-speed railway has achieved remarkable achievements all over the world. On August 1 of 2008, the first China high-speed railway, Beijing-Tianjin intercity railway, with a speed of 350 km/h was operated. By the end of 2018, the operation mileage of high-speed railway is 29,000 kilometers, accounted for more than 2/3 of the total mileage all over the world, and has transported more than 9 billion passengers. China has become the world's high-speed railway country with the longest operation mileage, the highest transport density, and the most complex operating scenarios.

In 2018, there are 2811 high-speed trains all over China. The average number of operating high-speed trains per day are 2186, the average operation mileage per day is 3.88 million kilometers, and the largest number of passengers per day reach 8.10 million, ranking first in the world. The data shows that high-speed trains have become main means of transportation for 1.3 billion Chinese people. From 2008 to 2018, the growth trend of the operating mileage, the total number of trains, the average operating number and the mileage of trains per day are shown in Fig.1. As it can be seen from the figure, the scale of China high-speed railway is steadily increased year by year, it will continue to expand in the future.

China is the country with the longest high-speed railway and the largest safe transportation of high-speed railway. ATP (Automatic Train Protection) system is the core system to guarantee the safe operation of high-speed trains. In each train, two sets of ATP system are located at both ends of the train. Through calculating the train speed profile, ATP determines the running speed, the position and the headway towards the preceding train, so as to protect the train from

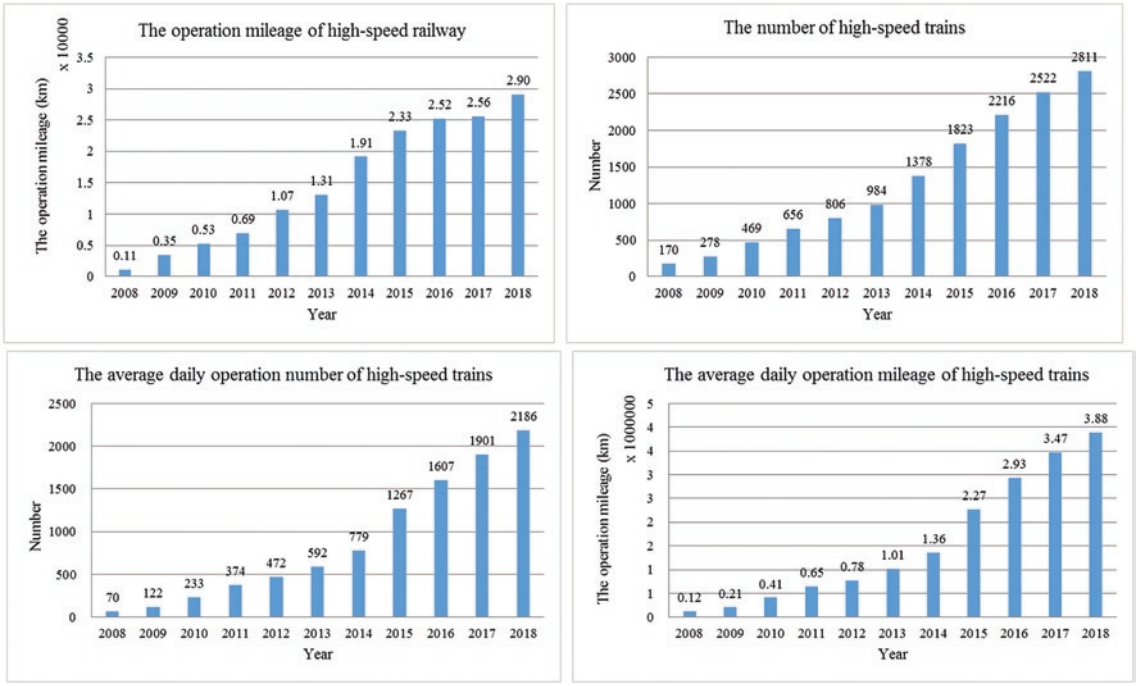

Fig.1. Growth trend of China high-speed railway scale

collision, derailment, and over-passing signals at danger. Therefore, the failure of ATP system will affect the safe operation of trains.

ATP system equipment includes VC (Vital Computer), SDP (Speed & Distance Processing unit), BTM (Balise Transmission Module), TCR (Track Circuit Reader), DMI (Driver-Machine Interface), TIU (Train Interface Unit), antenna, speed sensor, JRU (Juridical Recorder Unit), etc., where all devices cooperate with each other to guarantee the safe operation of train. As the scale of high-speed railway construction expands, the number of ATP systems is increasing. What's more, some ATP systems have been in operation for over 10 years, and a large number of ATP systems gradually enter the high-risk period over time. Therefore, better scientific maintenance strategies [11, 15] are urgently needed. However, there are still some deficiencies in application and maintenance of ATP systems.

Firstly, the maintenance strategy of ATP system is fixed and the maintenance mode is single. At present, China railway stipulates that ATP system should carry out planned maintenance in accordance with fixed maintenance intervals and items [5]. ATP system maintenance is divided into two different levels. The first is to maintain once a day on average, and the second is once a month on average. This mode will result in waste of maintenance resources or disrepair.

Secondly, the number of spare parts of ATP system are fixed. In order to replace and repair faulty equipment, China railway stipulates that each type of equipment of ATP system reserves spare parts in a fixed proportion [5], which influences maintenance owing to deficiencies and surplus of equipment. Since this mode can not balance the supply and demand well, it restricts the ability of emergency response.

Next, all kinds of ATP systems are maintained and configured in the same way, regardless of their failure rate. At present, there are five types of ATP systems in China, namely 300T, 300S, 300H, 200H and 200C. Different types of systems correspond to different production processes, design platforms, system structures, and software systems. Since their failure characteristics are different, so it should correspond to different maintenance strategies and reserve plans. However, there is only single way at present, which cannot dynamically adjust the maintenance strategy according to the equipment quality, or dynamically adjust the quantity of spare parts in a targeted manner. In such case, the equipment's safety capability is insufficient, and resources are not properly optimized.

Finally, the fixed maintenance strategy throughout the life cycle does not meet the inherent fault properties of the equipment. All ATP systems are maintained in the same strategy, regardless of service time, operation mileage, or natural environment. While, ATP equipment belong to electronic equipment, of which failure rate is a function of time, and the failure characteristics of the entire life cycle have obvious stages in line with the bathtub curve. The entire life cycle of ATP equipment can be divided into three phases: infant mortality, random failures, and wearout where each phase should correspond to elaborate maintenance strategy.

In order to solve the above problems, this paper proposes a method for intelligent forecasting failure rate of ATP system, which analyzes the characteristics of failure data and forecasts its short-term trend based on chaos from the perspective of history data. It can dynamically adjust the maintenance strategy and spare parts configuration in advance, and respond quickly to emergency situations, so as to prevent faults in advance and provide a strong guarantee for the safe operation of high-speed trains.

The rest of this paper is organized as follows. In section 2, the related work is reviewed. In section 3, the improved failure rate calculation method is proposed. In section 4, chaotic properties of ATP system failure rate series are determined. In section5, an intelligent prediction model is established. In section 6, the forecasting results are analyzed and applied. In section 7, the conclusion of our work is drawn.

2. Related work

The task of prediction is aimed at explicitly modeling variable dependencies and forecasting the next few values of a series [7]. On one hand, the failure rate of ATP system is affected by many factors such as service time, running mileage, natural environment, maintenance strategy, etc. So it is difficult to express influence mechanism with single functional relationship. On the other hand, ATP equipment belongs to the electronic device which is not separated from the common characteristics of the failure law, i.e., it contains inherent regular-

ity. Although the failure rate of ATP system shows great nonlinearity and seems to be irregular, it has a certain regularity.

Essentially, chaos is a nonlinear behavior existing between the realms of periodic and random [9]. Chaos theory extracts hidden regularity from the data directly to predict without subjective model [26]. Therefore, it is very suitable for analysis and research of ATP system failure rate.

The chaos theory itself has been studied. The research tries to sketch a theoretical view of chaos, i.e., to introduce chaotic and order properties, to compare them whenever possible, to find out how different a given order property and a given chaotic one are and to determine how convenient they are in the theory [2]. Besides, the research combines the Wiener chaos expansion approach to study the dynamics of a stochastic system with the classical problem of the prediction of a Gaussian process based on a realization of its past, to provide a general method for the construction [1].

On the other hand, chaos theory is used in the following aspects: analysis and prediction of short-term traffic flow [12, 29], railway freight traffic prediction [25, 31], big data analytic [23, 30] in intelligent transportation system and stock prediction [19]. It is used to analyze and predict certain relationships of transportation systems, which shows that in certain cases, fairly periodic systems analytically appear to be chaotic [9], and a soft computing approach and chaos theory have been successfully applied to solve the problem of early prediction of disruption in Joint European Torus machine [3]. The other study combines gradient descent method and chaos optimization method to predict leaching cycle period [18] and so on.

To summarize, the above researches provide a scientific and effective reference of data changes in the future. However, currently there is no research on failure rate forecasting of ATP system in China high-speed railway, and few literatures reported about intelligent maintenance from the perspective of prediction failure rate.

3. Improved failure rate calculation method

Failure rate in a quarter is used to measure the operation quality of different types of ATP systems in China railway. This evaluation index can explain the quality of systems to some extent. However, the failure of electronic devices has a cumulative effect. In other words, the device does not immediately fail when it is first put into use, and frequent failure is existing over time. Therefore, this paper uses the failure characteristics of electronic equipment, and adds cumulative effect factor to calculate the failure rate of ATP system based on existing calculation methods.

ATP system failure rate is one-dimensional time series:

$$x=\{x_i|i=1,2,\ldots,n\} \tag{1}$$

The existing failure rate is calculated as:

$$x_i=\frac{b_i}{r_i} \tag{2}$$

where x_i is the failure rate of a certain type of ATP system in the i-th quarter, b_i is the total number of faults of this type of ATP system in the i-th quarter all over the country, and r_i is the total operation mileage under the same conditions.

The improved failure rate is calculated as:

$$x_i=\frac{\sum_{j=1}^{i} a_j}{\sum_{j=1}^{i} s_j} \tag{3}$$

where x_i is the failure rate of a certain type of ATP system in the i-th day, a_j is the total number of faults of this type of ATP in the j-th day all over the country, and s_j is the total operation mileage on the same day and its unit is one million.

The existing method simply calculates the failure rate independently. Compared with it, the improved method proposed in this paper is obviously more scientific. It can be used as a key indicator to measure the quality of ATP system, but also to reconstruct the quality evaluation system fundamentally.

Firstly, it can be seen from equations (2) and (3) that with improved failure rate calculation method, time is refined and corrected from the original quarterly to daily. The calculation accuracy is higher.

Secondly, cumulative effects is added. The definition emphasizes the cumulative effect of ATP system over time, which reduces the fortuity of failure and better reflects the life cycle of the system.

What's more, since ATP system is powered on with the operation of high-speed trains, and powered off at the other time. Therefore, the accumulated operation time of ATP system is replaced by the accumulated operation mileage of high-speed trains, which can more accurately describe the characteristics of ATP system interval work.

4. ATP system failure rate series chaotic properties determination

Since one dimensional time series of ATP system failure rate is difficult to extract the potential failure regularity, so it should be mapped into high-dimensional space through phase space reconstruction theory, to determine whether it has chaotic properties. The SVM (Support Vector Machine) method [22] is used to train model in order to predict trends of ATP system failure in the short term. The whole idea is shown in Fig.2.

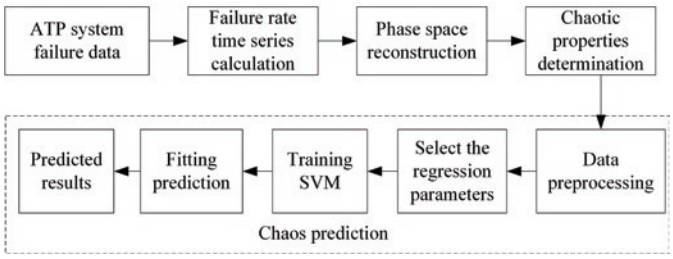

Fig. 2. The prediction flowchart of ATP system failure rate based on chaos

4.1. Original data collection and cleaning

Accurate collection of ATP failure data is the premise of failure rate prediction [16]. This paper obtains experimental sample data through the following steps.

1) Data collection and cleaning.

Firstly, collect fault conditions and operation mileage for each ATP system every day. The former includes time, location, summary, cause of the fault, and so on, and the latter includes start and end time, length of running, and so on. Then confirm that it is ATP system failure rather than the other systems failure through analysis and verification by professionals. i.e., the failure noise data is eliminated.

2) Determine the initial value.

In 2008, China high-speed railway started. In 2010, four types of ATP system, 300T-type, 300S-type, 200H-type, and 200C-type, were used on a large scale nationwide. Another 300H-type ATP system started to be used in large scale in 2013. Therefore, January 1 of 2010 is selected as the starting time point for failure data analysis. The data in the first three months after the specified starting time point is excluded since it has large fluctuations and error. Thus, the data from April 1, 2010 to December 31, 2018 is taken as a sample. The total

sample size is 3197, the training set sample size is 3047, and the test set sample size is 150. The sample size described below refers to the training set sample size, i.e., n=3047.

In units of days, xi is obtained in turn according to formula (3). The failure rate curve for each type of ATP system is shown in Fig.3.

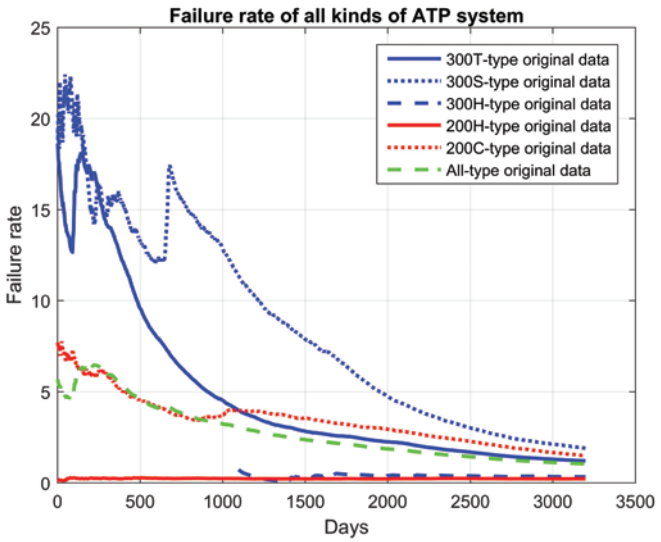

Fig. 3. Time series of all kinds of ATP system failure rate

In Fig.3, the ordinate represents the ATP system failure rate, and the green dotted line represents the failure rate for all types of ATP system. The following information can be obtained from Fig.3.

1) The failure rate shows overall downward trend and local fluctuations in a small range.

2) The system failure rates in 2010 and 2011 are significantly higher than in other years. The reasons are as follows: at the beginning of 2010, a variety of ATP systems have been used on a large scale for the first time, so the initial stability of system application is poor. In addition, China high-speed railway network system was still developing at that time, and its stability was relatively weak. Therefore, the failure rate is high. According to statistics, the number of ATP system failures in 2010 and 2011 accounted for 28.23% of the sum from 2010 to 2018, but the operation mileage only accounted for 7.36%, and the calculated failure rate was naturally slightly higher.

3) The 300H-type and 200H-type ATP systems are most stable with lowest failure rate.

In addition, it is very difficult to obtain other variation regularity of x. By extending one-dimensional time series [24] to the high-dimensional space, and guaranteeing the differential homeomorphism of the high-dimensional space and the original failure rate time series, the paper extracts the potential hidden regularity from high-dimensional space. Taken's embedding theorem [9, 31] shows that the geometrical features of ATP system failure rate time series are equal to the *m*-dimensional reconstruction space and have the same topology if there are appropriate delay time τ and embedded dimension *m*.

4.2. Phase space reconstruction

The one-dimensional time series *x* is reconstructed by delay embedded to obtain the trajectory matrix ***Y***:

$$Y=\begin{bmatrix} y_1 \\ y_2 \\ \cdots \\ y_{(m-1)\tau} \end{bmatrix}=\begin{bmatrix} x_1 & x_2 & \cdots & x_i & \cdots & x_{n-(m-1)\tau} \\ x_{1+\tau} & x_{2+\tau} & \cdots & x_{i+\tau} & \cdots & x_{n-(m-2)\tau} \\ \cdots & \cdots & \cdots & \cdots & \cdots & \cdots \\ x_{1+(m-1)\tau} & x_{2+(m-1)\tau} & \cdots & x_{i+(m-1)\tau} & \cdots & x_n \end{bmatrix} \quad (4)$$

where τ is delay time, and *m* is embedded dimension. Each column represents a phase point, and given $M=n-(m-1)\tau$, so ***Y*** is an $m\times M$ dimensional matrix.

The paper estimates delay time τ and embedded dimension *m* at the same time through C-C algorithm [20].

The time series *x* is subdivided into *t* disjoint time series [9] as following:

$$\{x(1), x(t+1), x(2t+1),\ldots\} \quad (5)$$

$$\{x(2), x(t+2), x(2t+2),\ldots\} \quad (6)$$

$$\{x(t), x(t+t), x(2t+t),\ldots\} \quad (7)$$

For each subseries, the statistic $S(m,n,r,\tau)$ is defined as following:

$$S(m,n,r,\tau)=\frac{1}{t}\sum_{l=1}^{t}\left\{C_l(m,n/t,r,\tau)-\left[C_l(1,n/t,r,\tau)\right]^m\right\} \quad (8)$$

where C_l is correlation integral of the *l* subseries, and its definition is:

$$C(m,n,r,\tau)=\frac{2}{M(M-1)}\sum_{1\le i<j\le M}\theta\left(r-\left\|X_i-X_j\right\|_\infty\right) \quad (9)$$

where *r* is neighbor radius, *M* is the number of phase points and θ(*) is Heaviside function.

Also, the distance of phase point X_i and the nearest phase point X_j is represented by infinite norm:

$$d=\left\|X_i-X_j\right\|_\infty=\max_{0\le k\le m-1}\left|x(i+k\tau)-x(j+k\tau)\right| \quad (10)$$

When $n\to\infty$, it can be written as:

$$S(m,r,\tau)=\frac{1}{t}\sum_{l=1}^{t}\left\{C_l(m,r,\tau)-\left[C_l(1,r,\tau)\right]^m\right\} \quad (11)$$

$S(m,r,\tau)\sim\tau$ reflect self-correlation of time series, and the paper takes improved C-C algorithm and defines:

$$\Delta S(m,\tau)=\text{std}\{S(m,r,\tau)\} \quad (12)$$

where std{*} represents mean square deviation of $S(m,r,\tau)$.

The values of *m* and *r* are estimated properly according to statistical theory. For $m=2,3,4,5$, $r_i=i\sigma/2$, $i=1,2,3$. where σ is mean square deviation of time series [28]. Define:

$$S(t)=\frac{1}{16}\sum_{m=2}^{5}\sum_{j=1}^{4}S(m,r,t) \quad (13)$$

$$\Delta S(t)=\frac{1}{4}\sum_{m=2}^{5}\Delta S(m,t) \quad (14)$$

$$S_{cor}(t) = \Delta S(t) + |S(t)| \tag{15}$$

The optimal delay time τ corresponds to the first minimum point of $\Delta S(t)$ and the optimal embedding window τ_w corresponds to the global minimum point of the $S_{cor}(t)$. Because of embedding window [20] $\tau_w=(m-1)\tau$, we can obtain embedded dimension m.

By the end of December 2018, there were 2,811 high-speed trains and 5,622 ATP systems in China railway, ranking first in the world. Among which, with the number of 2110, 300T-type is the largest and most representative ATP system, accounted for 37.53%. Therefore, the 300T-type ATP system failure rate one-dimensional time series x is selected as the input, and the delay time and embedded dimension are calculated as shown in Fig.4.

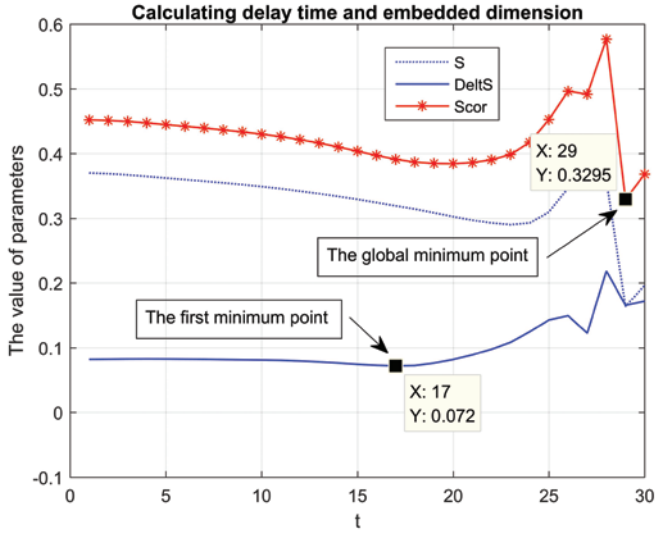

Fig. 4. Calculating delay time and embedded dimension by C-C algorithm

From Fig.4, the first minimum point of $\Delta S(t)$ is 17, so τ=17, and the global minimum point of the $S_{cor}(t)$ is 29, so τ_w=29, m=3.

Obtained delay time and embedded dimension, a size of 1×3047 one-dimensional time series x is reconstructed to 3×3013 high-dimensional matrix $\boldsymbol{Y}$.

4.3. Chaotic properties determination

It should be determined whether the series has chaotic properties after 300T-type ATP system failure rate time series x is reconstructed. The paper uses Lyapunov exponent method to judge chaotic properties. Grebogi [29] shows the system has chaotic properties as long as the maximum Lyapunov exponent λ is greater than 0.

The paper uses small data method to calculate the maximum Lyapunov exponent, and specific steps are as follows:

Step 1. Find the nearest neighbor $X_{\hat{j}}$ of phase point X_j in phase space, given:

$$d_j(0) = \min \left\| X_j - X_{\hat{j}} \right\|, \quad \left| j - \hat{j} \right| > P \tag{16}$$

where j=1,2,…M, and P represents the average cycle of time series. P is found by Fast Fourier Transformation, and P = 2.1145.

Step 2. Calculate the distance after phase point X_j evolution $i\Delta t$ time:

$$d_j(i) = \left| X_{j+i} - X_{\hat{j}+i} \right| \tag{17}$$

where i=1,2, …, min{M-j,M-$\hat{j}$}.

Step 3. Logarithm on both sides [29],

$$\ln d_j(i) \approx \ln d_j(0) + \lambda(i\Delta t) \tag{18}$$

The maximum Lyapunov exponent is the slope of the above straight line, it can be obtained approximately by the least squares method, i.e.:

$$y(i) = \frac{1}{q\Delta t}\sum_{j=1}^{q} \ln d_j(i) \tag{19}$$

where, q is the number of nonzero $d_j(i)$.

According to τ=17, m=3, the result of calculating the maximum Lyapunov exponent is shown in Fig.5.

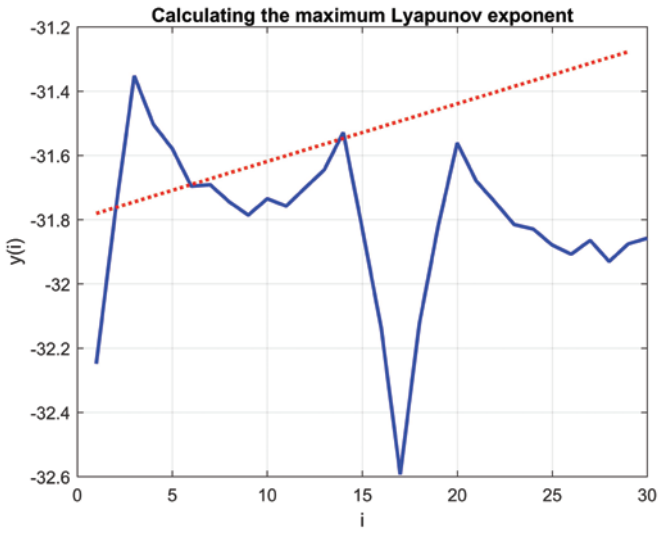

Fig. 5. Calculating the maximum Lyapunov exponent of 300T-type time series

In Fig.5, the solid line represents the value of $y(i)$, the dotted line indicates the line in step 3, whose slope is 0.018, namely the maximum Lyapunov exponent λ= 0.018 >0. Therefore, 300T-type failure rate time series has chaotic properties. It shows that the failure rate change of this ATP system follows certain rules, rather than irregular. The chaotic characteristics indicate that short-term predictions of failure rate can be made.

According to reference [25], the reciprocal of the maximum Lyapunov exponent (i.e., T=1/λ) represents the longest forecasting time of chaotic system. Because of λ=0.018, so T=1/λ≈56. It means that failure rate future 56 days can be predicated through 300T-type historical data. Therefore, it provides ample preparation time for the dynamic adjustment of maintenance strategy and spare parts configuration in advance. It also indicates that the intelligent prediction method proposed in this paper has the feasibility of implementation.

5. Intelligent prediction

After reconstructing the phase space and identifying the chaotic characteristics, the paper extracts potential failure regularity in a high-dimensional space, further to predict the trends and range of ATP system failure rate.

5.1. Prediction principle

300T-type failure rate time series $x=\{x_i|i=1,2,\ldots,n\}$ is made phase space reconstruction, and then it is obtained M phases point:

$$X(1)=\{x(1),x(1+\tau),\ldots, x(1+(m-1)\tau)\} \quad (20)$$

$$X(2)=\{x(2),x(2+\tau),\ldots, x(2+(m-1)\tau)\} \quad (21)$$

$$\ldots$$

$$X(M)=\{x(M),x(M+\tau),\ldots, x(M+(m-1)\tau)\} \quad (22)$$

Further evolution of phase points is:

$$X(M+1)=\{x(M+1),x(M+1+\tau),\ldots, x(M+1+(m-1)\tau)\} \quad (23)$$

The next sequence predict point $x(n+1)$ is exactly the element $x(M+1+(m-1)\tau)$.

There exists some definite and complex function connection between phase points $X(i)$ and $x(i+1+(m-1)\tau)$, namely:

$$x(i+1+(m-1)\tau)=f[X(i)] \quad (24)$$

Find an optimal function to fit $f[X(M_i)]$ with the SVM approximation ability [10], namely:

$$f[X(M_i)] = x(M_i+1+(m-1)\tau) \quad (25)$$

If it is determined $f(x)$, there:

$$x(n+1)=x(M+1+(m-1)\tau)=f[X(m)] \quad (26)$$

Similarly, it can forecast $x(n+2)$, $x(n+3)\ldots$

SVM is an effective machine learning method based on statistical learning theory, and has excellent learning performance and strong generalization ability [17, 27]. This paper needs to determine the function $f(x)$, which is clearly a regression problem. ε-support vector regression(ε-SVR) belongs to SVM and its goal of training is:

$$|y-f(x)|\leq\varepsilon \quad (27)$$

If specify the insensitivity ε, then get ε-SVR, i.e.:

$$\min_{w,b,\xi}\left[\frac{1}{2}\|w\|_2^2+c\sum_{i=1}^{l}\left(\xi_i+\xi_i^*\right)\right] \quad (28)$$

$$s.t. \quad y_i-\left\{\left[w,\Phi(x_i)\right]-b\right\}\leq\varepsilon+\xi_i \quad (29)$$

$$y_i-\left\{\left[w,\Phi(x_i)\right]-b\right\}\geq-\varepsilon-\xi_i^* \quad (30)$$

$$\xi_i\geq 0,\xi_i^*\geq 0, i=1,2,\cdots,l \quad (31)$$

Its solution is:

$$f(x)=\sum_{i=1}^{l}(a_i-a_i^*)K(x,x_i)-b \quad (32)$$

where c is the penalty coefficient and other parameters are available from references [13, 21]. So far, the model of intelligent forecasting of ATP system failure rate by chaos is shown in Fig.6.

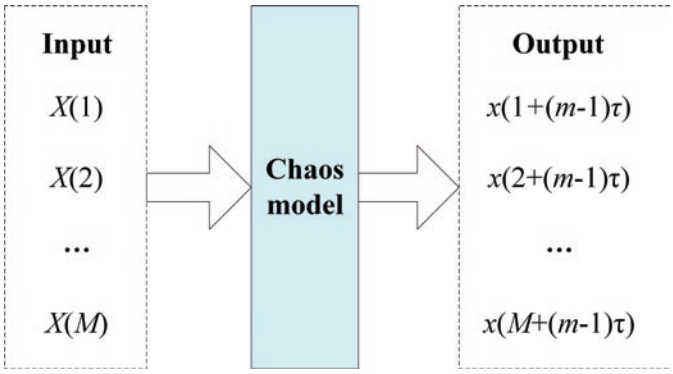

Fig.6. The model of intelligent forecasting of ATP system failure rate

5.2. Data normalization process

300T-type ATP system failure rate time series is reconstructed to $m\times M$ dimensional matrix $\boldsymbol{Y}$, i.e., the size of training set is 3×3013.

Select $(X(1),X(2),\ldots,X(M))$ as training set, that is X_train=$(X(1),X(2),\ldots,X(3013))$.

Select $(X(1),X(2),\ldots,X(M-1))$ as training set feature, that is X_train_ feature =$(X(1),X(2),\ldots,X(3012))$.

Select $(x(2+(m-1)\tau), x(3+(m-1)\tau), \ldots,x(n))$ as training set label, that is X_train_ label =$(x(36), x(37), \ldots,x(3047))$.

Early tentatively forecasting shows that the accuracy is low regarded matrix $\boldsymbol{Y}$ as an input directly without making data processing. Thus, training set feature and label are made normalization preprocessing according to the following map:

$$f: x\rightarrow y=\frac{x-\min(x)}{\max(x)-\min(x)} \quad (33)$$

In order to improve prediction accuracy, the element of matrix $\boldsymbol{Y}$ as chaos model input is structured into the range [0,1].

5.3. Model optimal parameters selection

The advantages and disadvantages of each parameter should be comprehensively considered to train the prediction model. To complement and balance the multiple parameters, optimal model is achieved. The training model parameter evaluation indicators are as follows:

Mean Square Error (MSE):

$$MSE=\frac{1}{n}\sum_{i=1}^{n}\left[f(x_i)-y_i\right]^2 \quad (34)$$

Squared Correlation Coefficient (r^2):

$$r^2=\frac{\left[n\sum_{i=1}^{n}f(x_i)y_i-\sum_{i=1}^{n}f(x_i)\sum_{i=1}^{n}y_i\right]^2}{\left(n\sum_{i=1}^{n}f(x_i)^2-\left(\sum_{i=1}^{n}f(x_i)\right)^2\right)\left(n\sum_{i=1}^{n}y_i^2-\left(\sum_{i=1}^{n}y_i\right)^2\right)} \quad (35)$$

where n represents the number of samples.

It needs to determine the three parameters [4, 8] for solving regression problems of $f(x)$ using SVR, which are insensitivity ε, penalty coefficient c and kernel parameter g.

The paper selects radial basis function:

$$K(x,y)=\exp\left(-g\left\|x-y\right\|^2\right) \tag{36}$$

where g is kernel parameter [6, 14].

First of all, set insensitivity ε=0.01. Then find the best c and g within the scope of the index of 2 by a cross validation method.

Roughly determine the scope of optimization c and g, and the values c are 2^{-6},2^{-5},…,2^{6}, and the values g are 2^{-6},2^{-5},…,2^{0}. The rough selection results are shown in Fig.7. Where the best c=0.25, g=1, and the minimum MSE=0.0038507.

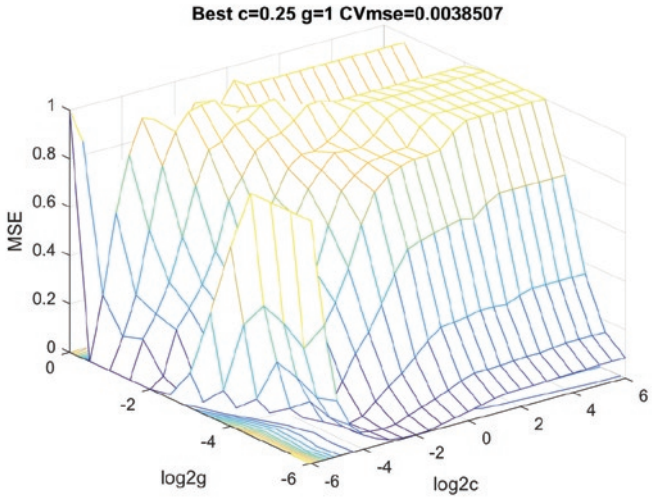

Fig. 7. Rough selection results of parameters c and g

In Fig.7, x-axis represents the value of 2 of c power, and y-axis represents the value of 2 of g, while z-axis represents mean square error under corresponding c and g.

In order to find a better parameter value, the value range of the penalty coefficient c is reduced to 2^{-6}~2^{-2}, and the range of the kernel parameter g is expanded to 2^{-6}~2^{2}. Thus, fine selection results of parameters c and g are shown in Fig.8. Where the best c=0.125, g=2, and the minimum MSE=0.003488. The minimum MSE, reduced by 9.42%, is less than the one by rough selection, indicating that the parameter results by fine selection are better.

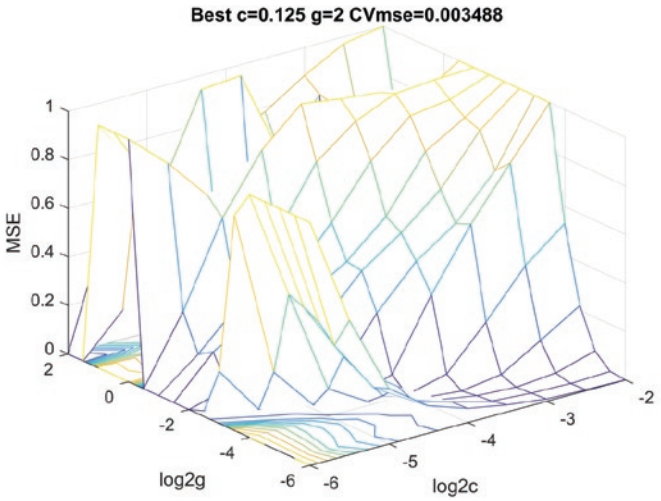

Fig. 8. Fine selection results of parameters c and g

5.4. Forecasting results

To train SVR according to the best parameters c and g in Fig.8, a regression model to fit $f(x)$ can be obtained based on the input-output relationship of Fig.6. Then the trend of future failure rate of 300T-type ATP system is predicted. At last, to set the predicted step length as 100, the model accuracy is verified. Fig.9 is a comparison between chaos forecasting data and the original data.

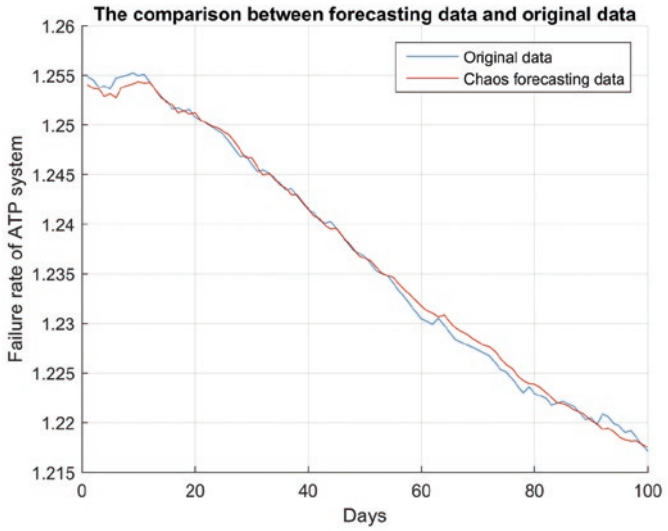

Fig. 9. The comparison between chaos forecasting data and the original data

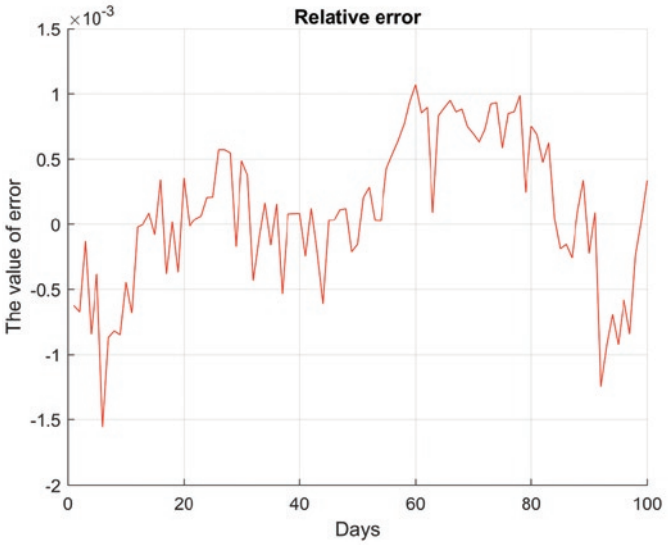

Fig. 10. Relative error of chaos prediction

In Fig.9, the data of chaos prediction and the original data are consistent, Mean Square Error MSE=0.0003416, Squared Correlation Coefficient r^2=0.997092, that is, the prediction accuracy reaches 99.71%. The relative error of chaos prediction is shown in Fig.10. The

error is relatively concentrated in the interval [-0.001, 0.001], which indicates that the chaos method is suitable for the failure rate trend prediction of ATP system in China high-speed railway.

6. Forecasting results analysis

This section analyzes the effectiveness of the proposed intelligent prediction method of failure rate from two aspects: model prediction accuracy and prediction results application.

6.1. Model prediction accuracy analysis

To illustrate the effectiveness of chaos intelligent forecasting on ATP system failure rate, this paper compares chaos forecasting results with the results of SVR method. The main differences between two methods are: chaos prediction makes the matrix $\boldsymbol{Y}$ as an input after phase space reconstruction, while SVR prediction makes one-dimensional time series x as an input directly; in addition, the former processing objects are phase points of high- dimensional matrix, while the latter are elements of one-dimensional time series. The main differences between the two methods are shown in Table 1.

The SVR prediction model still takes the 300T-type ATP system failure rate time series x as a sample, taking ε=0.01, and the 100 data as the test sets. Select the best parameter c=0.0442, g=5.6569, correspondingly, the minimum MSE=0.0041.

The mean squared error and squared correlation coefficient of chaos and SVR model are respectively shown in Table 2.

It can be seen from Table 2 that for the same 300T-type failure rate time series, chaos prediction mean square error is smaller than SVR prediction, while the former squared correlation coefficient is bigger than the latter, showing that chaos prediction accuracy is higher than the SVR.

In addition, the equipment failure rate is closely related to the quality of product, and the original quality determines the level of failure rate to a large extent, which coincides with the essential characteristics of the chaotic system's sensitivity to the initial value. It shows that the experimental results are consistent with the actual situation.

In summary, compared with SVR prediction, the prediction of the failure rate of ATP system based on chaos theory is more suitable and more accurate.

6.2. Analysis of the forecasting results application

Maintenance strategies and configure spare parts can be dynamically adjusted based on the volatility of forecasting results.

If the predicted failure rate is in upward trend, the frequency of maintenance should be increased, the maintenance items should be extended, and the equipment with higher failure rate should be overhauled to prevent the failure. At the same time, the spare parts of system should be adequately configured in advance to improve the emergency response capacity.

If the predicted failure rate is in a downward trend, the frequency of maintenance can be appropriately decreased, and the maintenance items can be simplified, which can reduce the workload of maintenance and alleviate the contradiction between insufficient and excessive reserves.

Therefore, the intelligence of the failure rate prediction method proposed in this paper is reflected in the following aspects:

1) For different types of ATP systems, to dynamically adjust different targeted maintenance strategies and spare parts reserve plans.

2) For a specific type of ATP system, to dynamically adjust maintenance intervals and items.

3) For a specific type of ATP system, to dynamically configure the quantity of spare parts.

4) For a set of ATP system, maintenance plans throughout the life cycle are dynamically adjusted based on factors such as service time, operation mileage, and natural environment and so on.

In summary, the differences between before and after using the intelligent prediction method presented in this paper are shown in Table 3.

Table 1. Difference between chaos model and SVR model

Difference point	Chaos model	SVR model
Processing objects	High- dimensional matrix $\boldsymbol{Y}$	One-dimensional time series x
Training set feature	$X(1),X(2),\ldots,X(M\text{-}1)$	$x(1),x(2),\ldots,x(n)$
Training set label	$x(2+(m\text{-}1)\tau), x(3+(m\text{-}1)\tau), \ldots,x(n)$	Day number sequence,1: n
One-step prediction	$X(M+1)$	$x(n+1)$

Table 2. Forecasting results comparison of chaos and SVR

Difference point	Chaos model	SVR model
MSE	0.0003416	0.0984576
r^2	0.997092	0.877012

Table 3. Using intelligent prediction methods before and after comparison

Difference point	Before the novel method	After the novel method
Maintenance strategy	Fixed maintenance cycle and content.	Dynamic maintenance cycle and content.
Spare parts reserve	The quantity is fixed.	The quantity is dynamic.
Maintenance strategy for different types of ATP systems	The same way.	The different way.
Spare parts reserve method for different types of ATP systems	The same way.	The different way.

7. Conclusion

On the basis of existing quality evaluation methods, this paper added the cumulative effect of electronic equipment over time, and improved the quality evaluation system of ATP system in China high-speed railway. By calculating the maximum Lyapunov exponent, it was revealed that failure rate change of ATP system had chaotic characteristics, in which it proved that ATP system failure rate time series was extremely sensitive to the initial conditions. Then a short-term intelligent prediction model of failure rate based on chaos was established, and the real failure data from 2010 to 2018 was selected as a sample for simulation experiments. The results showed that the accuracy of the intelligent prediction model was 99.71%, much higher than SVR prediction model.

According to the results, the dynamic adjustment to maintenance strategy and dynamic reserve spare parts were realized, and the personalized maintenance strategy of each ATP system through full life cycle was established. What's more, it improved the existing single and fixed maintenance mode of China railway, and solved the pain points such as rough maintenance mode, unbalanced supply and demand of spare parts, and insufficient emergency response capability. Finally, it realized the intelligent maintenance of ATP system in China high-speed railway.

As future work, the authors propose to explore the following research lines: (1) To further analyze the complex relationship among the failure rate, the natural environment, maintenance strategy and operation mileage and so on. (2) If there are more detailed classification of spare parts data, the method can make particular forecasting, to provide a reasonable reserves and maintenance strategy for a special spare parts.

Acknowledgements

This work was supported by State Key Laboratory of Rail Traffic Control and Safety under Grants RCS2018ZT010, by China Academy of Railway Sciences under Grants 2017YJ056, by Nanning special funds for small and high talents under Grants 2017042 and 2017043, by upgrading of basic ability of young and middle-aged teachers in Colleges and universities in Guangxi under Grants 2018KY0747 and 2018KY0748. The authors would like to thank Miss Junli Li, she revised grammatical and syntactical errors in the manuscript.

References

1. Alpay D, Kipnis A. Wiener Chaos Approach to Optimal Prediction. Numerical Functional Analysis and Optimization 2015; 36(10): 1286-1306, https://doi.org/10.1080/01630563.2015.1065273.
2. Blanchard F. Topological chaos: what may this mean. Journal of Difference Equations and Applications 2009; 15(1): 23-46, https://doi.org/10.1080/10236190802385355.
3. Cacciola M, Costantino D, Morabito F-C, Versaci M. Soft Computing and Chaos Theory for Disruption Prediction in Tokamak Reactors. International Journal of Modelling and Simulation 2008; 28(2): 165-173, https://doi.org/10.1080/02286203.2008.11442464.
4. Cao S-C, et al. Establishing a Flight Load Parameter Identification Model with Support Vector Machine Regression. Journal of Northwestern Polytechnical University 2013; 31(4): 535-539.
5. China railway standard. CTCS-2/3 Level Train Control on-board Equipment Maintenance Management Measures 2015; tiezongyun 57.
6. Dai A-N, et al. Intelligent control of a grain drying system using a GA-SVM-IMPC controller. Drying Technology 2018; 36(12): 1413-1435, https://doi.org/10.1080/07373937.2017.1407938.
7. Esling P, Agon C. Time-Series Data Mining. ACM Computing Surveys 2012; 45(1): 12-34, https://doi.org/10.1145/2379776.2379788.
8. Feng X-X, et al. Adaptive Multi-Kernel SVM With Spatial-Temporal Correlation for Short-Term Traffic Flow Prediction. IEEE Transactions on Intelligent Transportation Systems (Early Access) 2018: 1-13.
9. Frazier C, Kockelman M. Chaos Theory and Transportation Systems. Journal of the Transportation Research Board 2004; 1897: 9-17, https://doi.org/10.3141/1897-02.
10. Fu G, et al. Short-term Traffic Flow Forecasting Model Based on Support Vector Machine Regression. Journal of South China University of Technology(Natural Science Edition) 2013; 41(9): 71-76.
11. Galar D, Gustafson A, Tormos B, Berges L. Maintenance Decision Making based on different types of data fusion. Eksploatacja i Niezawodnosc - Maintenance and Reliability 2012; 14 (2): 135-144.
12. Ghosh B, Basu B, O'Mahony M. Multivariate Short-Term Traffic Flow Forecasting Using Time-Series Analysis. IEEE Transactions on Intelligent Transportation Systems 2009; 10(2): 246-254, https://doi.org/10.1109/TITS.2009.2021448.
13. Guo Y-M, Ran C-B, Li X-L, Ma J-Z, Zhang L. Weighted prediction method with multiple time series using multi-kernel least squares support vector regression. Eksploatacja i Niezawodnosc - Maintenance and Reliability 2013; 15 (2): 188-194.
14. Guo Y-M, Wang X-T, Liu C, Zheng Y-F, Cai X-B. Electronic system fault diagnosis with optimized multi-kernel SVM by improved CPSO. Eksploatacja i Niezawodnosc - Maintenance and Reliability 2014; 16 (1): 85-91.
15. Jimenez Cortadi A, Irigoien I, Boto F, Sierra B, Suarez A, Ga lar D. A statistical data-based approach to instability detection and wear prediction in radial turning processes. Eksploatacja i Niezawodnosc - Maintenance and Reliability 2018; 20 (3): 405-412, https://doi.org/10.17531/ein.2018.3.8.
16. Kozielski M, Sikora M, Wróbel Ł. Decision support and maintenance system for natural hazards, processes and equipment monitoring. Eksploatacja i Niezawodnosc - Maintenance and Reliability 2016; 18 (2): 218-228, https://doi.org/10.17531/ein.2016.2.9.
17. Liu B-L, et al. An improved PSO-SVM model for online recognition defects in eddy current testing. Nondestructive Testing and Evaluation 2013; 28(4): 367-385, https://doi.org/10.1080/10589759.2013.823608.
18. Liu C, Wu A-X, Yin S-H, Chen-X. Nonlinear chaotic characteristic in leaching process and prediction of leaching cycle period. Journal of Central South University 2016; 23(16): 2935-2940, https://doi.org/10.1007/s11771-016-3357-9.
19. Ma J-H, Qi E-S, Mo X. Application Study on Reconstruction of Chaotic Time Series and Prediction of Shanghai Stock Index. Systems Engineering-Theory & Practice 2013; 23(12): 86-93.
20. Meng Y-Y, Lu J-P, Wang J. Wind Power Chaos Prediction Based on Volterra Adaptive Filter. Power System Protection and Control 2012; 40(4): 90-95.

21. Nicolas P-C, Theodore B-T. On-line SVM learning via an incremental primal-dual technique. Optimization Methods & Software 2013; 28(2): 256-275, https://doi.org/10.1080/10556788.2011.633705.
22. Qu X, Wang W, Wang W-F, Liu P. Real-time rear-end crash potential prediction on freeways. Journal of Central South University 2017; 24(11): 2664-2673, https://doi.org/10.1007/s11771-017-3679-2.
23. Świderski A, Jóźwiak A, Jachimowski R. Operational quality measures of vehicles applied for the transport services evaluation using artificial neural networks. Eksploatacja i Niezawodnosc - Maintenance and Reliability 2018; 20 (2): 292-299, https://doi.org/10.17531/ein.2018.2.16.
24. Vališ d, Koucky M, Zak L. On approaches for non-direct determination of system deterioration. Eksploatacja i Niezawodnosc - Maintenance and Reliability 2012; 14 (1): 33-41.
25. Wu H-W, Wang F-Z. Research on Railway Freight Traffic Prediction Based on Maximum Lyapunov Exponent. Journal of the China Railway Soci 2014; 36(4): 8-13.
26. Wu X-X. Li-Yorke chaos of translation semigroups. Journal of Difference Equations and Applications 2014; 20(1): 49-57, https://doi.org/10.1080/10236198.2013.809712.
27. Yan Z-G, Yao K, Yang Y-X. A novel adaptive differential evolution SVM model for predicting coal and gas outbursts. Journal of Difference Equations and Applications 2017; 23(1-2): 238-248, https://doi.org/10.1080/10236198.2016.1214725.
28. Zhang H-B, Sun X-D, He Y-L. Analysis and Prediction of Complex Dynamical Characteristics of Short-term Traffic Flow. Acta Physica Sinica 2014; 63(4): 1-8.
29. Zhang Y-M, Wu X-J, Bai S L. Chaotic Characteristic Analysis for Traffic Flow Series and DFPSOVF Prediction Model. Acta Physica Sinica 2013; 62(19): 1-9.
30. Zhu L, Yu F-R, Wang Y-G, et al. Big Data Analytics in Intelligent Transportation Syetems: A Survey. IEEE Transactions on Intelligent Transportation Systems 2019; 20(1):383-398, https://doi.org/10.1109/TITS.2018.2815678.
31. Zhu Z-H, Weng Z-S. Railway Passenger and Freight Volume Forecasting Based on Chaos Theory. Journal of the China Railway Soci 2011; 33(6): 1-7.

Renwei KANG
Junfeng WANG
State Key Laboratory of Rail Traffic Control and Safety
Beijing Jiaotong University
Haidian, Beijing 100044, China

Jianfeng CHENG
Signal & Communication Research Institute
China Academy of Railway Sciences
Haidian, Beijing 100081, China

Jianqiu CHEN
Yanzhi PANG
Rail Transit Scientific Research Institution
Nanning University
Nanning 530200, Guangxi, China

E-mails: krwjob@126.com, w2881@163.com, 583735920@qq.com, chenjq@bjtu.edu.cn, pangyanzhi@126.com

Article citation info:
JAMROZIAK K, KWASNIOWSKI S, KOSOBUDZKI M, ZAJAC P. Analysis of heat exchange in the powertrain of a road vehicle with a retarder. Eksploatacja i Niezawodnosc – Maintenance and Reliability 2019; 21 (4): 577–584, http://dx.doi.org/10.17531/ein.2019.4.6.

Krzysztof JAMROZIAK
Stanislaw KWASNIOWSKI
Mariusz KOSOBUDZKI
Pawel ZAJAC

ANALYSIS OF HEAT EXCHANGE IN THE POWERTRAIN OF A ROAD VEHICLE WITH A RETARDER

ANALIZA WYMIANY CIEPŁA W UKŁADZIE NAPĘDOWYM POJAZDU DROGOWEGO Z RETARDEREM

The paper presents a heat exchange model for the cooling system of any complex, physical system. Verification of the correctness of the theoretical model was carried out on the example of a vehicle with a combustion engine and additionally equipped with a hydraulic retarder. The results of laboratory tests, which were carried out on an engine test bench, were also performed for the above mentioned powertrain, so as to compare the results of modelling with the results of the tests. Determining the operating parameters of the components of the cooling system aimed at protecting the entire powertrain against overheating is a key task. Theoretical analysis of heat exchange in the powertrain of a road vehicle was carried out, with particular emphasis on the hydraulic retarder (a device braking the vehicle during a descent on roads with a high gradient of the road, mandatory according to the ADR convention). The subject of the study was a mathematical model of a complex cooling system developed by the authors, described by means of balance equations and differential equations. This model was tested with the use of the Matlab-Simulink suite for given load parameters of the cooling system, which were used in tests on an engine test bench. The values of coefficients describing the thermal state of the powertrain were obtained. Simulations were performed for different variants of technical parameters of the expanded cooling system. In this way, individual units and components of the cooling system were optimized so that it fulfilled its role in the assumed operating conditions and the ecologization of emission of energy sources (fuel) and harmful substances.

Keywords: *heavy-duty vehicle operation, vehicle retarder, brake support, heat exchange.*

Praca zawiera model wymiany ciepła układu chłodzenia dla złożonego, dowolnego układu fizycznego. Weryfikację poprawności modelu teoretycznego przeprowadzono na przykładzie pojazdu z silnikiem spalinowym oraz dodatkowo wyposażonym w retarder hydrauliczny. Wyniki badań laboratoryjnych, które przeprowadzono na hamowni również wykonano dla w/w zespołu napędowego, tak aby porównać wyniki modelowania z wynikami badań. Ustalenie parametrów eksploatacji elementów układu chodzenia, którego celem jest zabezpieczenie całego układu napędowego przed przegrzaniem to kluczowe zadanie. Przeprowadzono teoretyczną analizę wymiany ciepła w układzie napędowym pojazdu drogowego ze szczególnym uwzględnieniem zwalniacza hydraulicznego (urządzenia hamującego pojazd podczas zjazdu na drogach o dużym pochyleniu jezdni, obowiązkowe wg konwencji ADR). Przedmiotem badań był opracowany przez autorów model matematyczny rozbudowanego układu chłodzenia opisany za pomocą równań bilansowych i równań różniczkowych. Model ten testowano z wykorzystaniem pakietu Matlab-Simulink dla zadanych parametrów obciążenia układu chłodzenia, które wykorzystywano w badaniach w stanowiskowych na hamowni silnikowej. Uzyskano wartości współczynników opisujących stan cieplny jednostki napędowej. Symulacje wykonano dla różnych wariantów parametrów technicznych rozbudowanego układu chłodzenia. W ten sposób optymalizowano poszczególne zespoły i podzespoły układu chłodzenia, tak aby spełniał on swoją rolę w zakładanych warunkach eksploatacji i ekologizację emisji źródeł energii (paliwa) i szkodliwych substancji.

Słowa kluczowe: *użytkowanie pojazdów ciężkich, zwalniacz pojazdu, wspomaganie hamowania, wymiana ciepła.*

1. Introduction

Modern trucks for the transport of cargo/humans, apart from the conventional braking system, are equipped with additional braking systems which can take the form of an electrodynamic brake, engine brake or hydraulic brake [5, 9, 10, 12]. When driving on long and steep road sections, the vehicle often uses the service brake, which can lead to increased heat load and serious wear to the brake system. This is a dangerous phenomenon affecting the decrease in the efficiency of the mechanical brake due to the thermal recession of the system [3, 4, 28]. Hydraulic retarders, commonly used in commercial vehicles, are auxiliary devices that can reduce vehicle speed by converting the vehicle's mechanical energy into heat energy absorbed by the retarder's working medium that is oil.

Compared to other auxiliary equipment, hydraulic retarders have many advantages such as low weight, high braking torque, long operating hours, good thermal diffusivity and zero environmental pollution. The design and principle of operation of hydraulic retarders/intarders in the literature is quite well described [14, 23, 24]. Nevertheless, the development of new technologies affects the efficiency

of these devices and their characteristics are being investigated by many researchers [18, 26, 35]. It is noted that they are mandatory in Europe for vehicles with a gross vehicle weight (GVW) of over 16 tones. Currently, they are also installed in vehicles with smaller GVW parameters [8]. These units are characteristic heat exchangers, the maintenance of which at the required level of efficiency also depends on the powertrain cooling system's capacity [17, 25, 29, 38]. Operation of the hydraulic retarder is periodic and its cooling system is connected to the cooling system of the traction engine.

The capacity of the cooling system must be selected in such a way as to meet the assumed operating conditions of the truck. When considering the thermal capacity of the mass of the powertrain and the efficiency of the cooling system, the thermal capacity received from the retarder over a period of 12 minutes of its operation shall be estimated. This time has been estimated on the basis of average downward slopes existing on the European roads [24]. This requires designers to develop efficient equipment.

Great emphasis was placed on modelling traction performance characteristics versus technical parameters and geometry of rotating elements of the retarder [6, 13, 30], as well as testing the medium flow field structure [23, 27]. Numerous studies have been devoted to mathematical modelling in the analyses of the effect of rotor speed and fill ratio on retarder output torque [15, 31, 32, 33, 34]. Mathematical models are based on complex differential equations of flows, which are often solved using numerical methods [12, 21, 36]. With the use of numerical models in computer simulations it is possible to make certain verifications of the flow rate or the average speed of the working fluid, as well as the braking torque - which was the subject of papers [1, 2, 20, 22]. In the analyzed literature [11, 19, 35, 37], the majority of problems concern the evaluation of retarders efficiency and their optimization, while the influence of the design heat output of the radiator on the braking efficiency of hydraulic retarder was rather simplified. Taking into account the design thermal capacity of the radiator in the coupled system of hydraulic retarder cooling system, main engine cooling system and engine oil cooling system, a detailed assessment of the thermal capacity of these units is required. Each of the mentioned devices is filled with a cooling medium with different thermo-physical properties. The entire system works correctly if none of the cooling media exceeds the permissible operating temperatures [24, 29].

The authors of this paper focused their attention on estimating the capacity of the main powertrain radiator, assuming that its efficiency can be reduced to about 15% due to local obstructions and contamination of the system. The aim of this paper is to select a main radiator working with multiple sub-systems and a hydraulic retarder. Achievement of the goal required the authors to develop a mathematical model, which was subject to simulation verification for two refrigerating media. The effects of ambient temperature, the volume of liquid in the retarder system, the size of the engine main radiator and the pump capacity in the cooling system on the temperature level of cooling media were analyzed. On the basis of the conducted tests and the obtained results, the direction of optimization of the adopted cooling system was indicated so that it complies with the requirements [7] under the assumed operating conditions. The obtained heat exchange coefficients were verified on a test stand, using the example of the 6C107[1] engine.

The presented calculations are only an example of how this model can be used for practical purposes, the versatility of which lies in the possibility of extending the powertrain cooling system with specific components.

2. Characteristics of the operating conditions of the vehicle under analysis

For the analytical tests, a propulsion system of a road vehicle powered by a diesel engine type 6C107, with a capacity of 6.53 dm^3 and power of 92.5 kW/2600 rpm, produced in Poland, was adopted [33]. It was assumed that the vehicle is equipped with a Voith R120-4 hydraulic retarder. The data of this retarder were used to estimate the coefficients characterizing the heat exchange in this device [27, 31]. The structure of the cooling system to be tested is illustrated in Fig. 1.

The engine cooling system was protected by a bellows thermostat with the characteristics shown in Fig. 2 [34].

During the simulation tests it was assumed that the vehicle was driving on a horizontal road, emitting energy into the cooling system in the amount of q_{dost} = 29.5 kW. After 50 minutes, the vehicle starts to descend on a gradient of i = 7%. The descent lasts 12 minutes. The vehicle then continues to run on flat ground. The initial time of

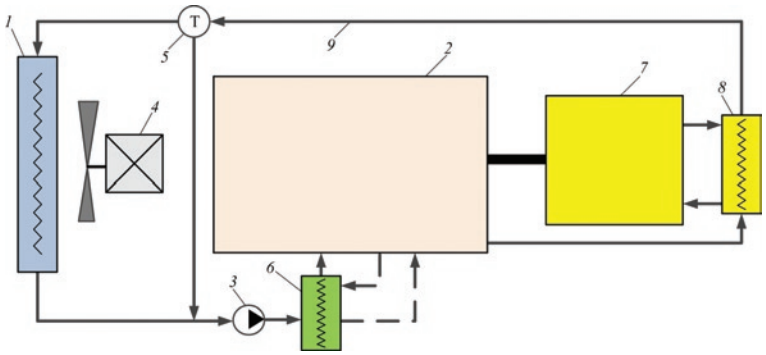

Fig. 1. Structure of the cooling system of a road vehicle powertrain equipped with a retarder: 1 – liquid-air cooler, 2 – engine, 3 – circulation pump of cooling liquid, 4 – fan of the cooler with electric drive, 5 – thermostat, 6 – engine oil cooler, 7 – retarder, 8 – retarder cooler, 9 – ducts

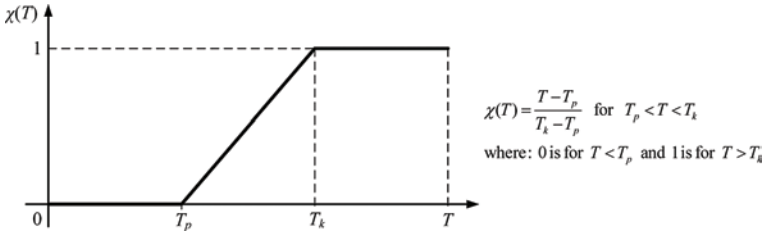

Fig. 2. Characteristics of the bellows thermostat for engine protection 6C107, where T_p – temperature at the beginning of thermostat opening, T_k – temperature of full thermostat opening

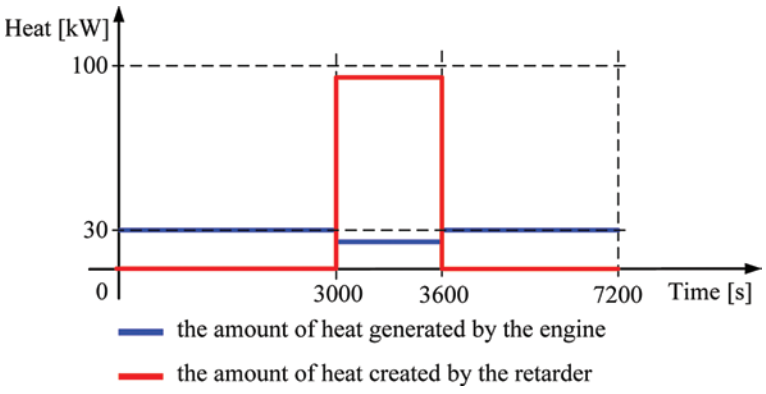

Fig. 3. Trend of thermal loads in the powertrain of the vehicle under analysis

1 The 6C107 engine is a design developed based on 400 Leyland

50 minutes of constant speed driving causes the temperatures in the engine cooling system to be close to asymptotic levels under the assumed operating conditions [36, 39]. The trend of thermal loads in the cooling system of the powertrain was assumed as shown in Fig. 3.

3. Powertrain heat exchange model

A diagram of the powertrain model is shown in Figure 4.

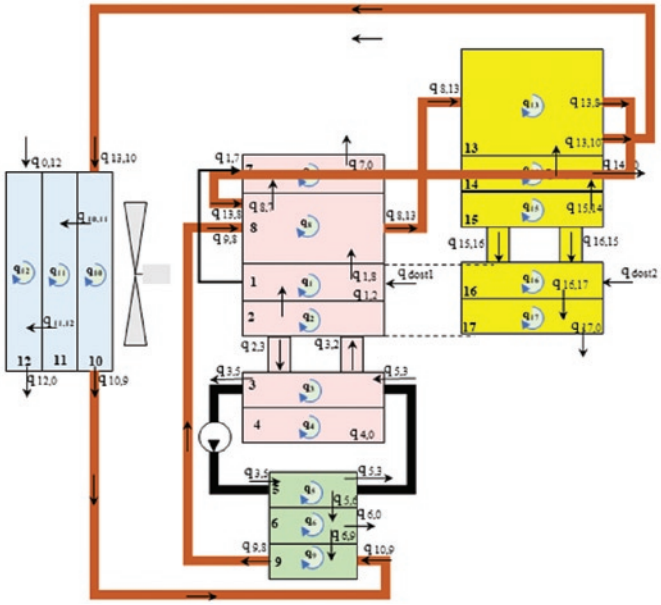

Fig. 4. Block diagram of engine with water-air cooler, engine oil cooler, retarder and thermostat; where: 0 – ambient environment, 1 – hot engine components, 2 – oil in the engine block, 3 – oil in the oil sump, 4 – oil sump, 5 – oil in the oil cooler, 6 – body of the oil cooler, 7 – engine body, 8 – water in the engine block, 9 – water in the oil cooler, 10 – water in the main cooler, 11 – body of the main cooler, 12 – water in the retarder cooler, 13 – water in the retarder cooler, 14 – body of the retarder cooler, 15 – retarder oil in the cooler, 16 – retarder oil in the retarder, 17 – retarder body

The thermal balance of the model is described by the following equations:

$$q_1 = q_{dost1} - q_{1,2} - q_{1,7} - q_{1,8} \tag{1}$$

$$q_2 = q_{1,2} + q_{3,2} - q_{2,3} \tag{2}$$

$$q_3 = q_{3,2} + q_{5,3} - q_{3,2} - q_{3,5} - q_{3,4} \tag{3}$$

$$q_4 = q_{3,4} - q_{4,0} \tag{4}$$

$$q_5 = q_{3,5} - q_{5,3} - q_{5,6} \tag{5}$$

$$q_6 = q_{5,6} - q_{6,0} - q_{6,9} \tag{6}$$

$$q_7 = q_{1,7} + q_{8,7} - q_{7,0} \tag{7}$$

$$q_8 = q_{1,8} + q_{9,8} + q_{13,8} - q_{8,7} - q_{8,13} \tag{8}$$

$$q_9 = q_{6,9} + q_{10,9} - q_{9,8} \tag{9}$$

$$q_{10} = q_{13,10} - q_{10,11} - q_{10,9} \tag{10}$$

$$q_{11} = q_{10,11} - q_{11,12} \tag{11}$$

$$q_{12} = q_{11,12} + q_{0,12} - q_{12,0} \tag{12}$$

$$q_{13} = q_{14,13} + q_{8,13} - q_{13,10} - q_{13,8} \tag{13}$$

$$q_{14} = q_{15,14} - q_{14,13} - q_{14,0} \tag{14}$$

$$q_{15} = q_{16,15} - q_{15,16} - q_{15,14} \tag{15}$$

$$q_{16} = q_{dost2} + q_{15,16} - q_{16,15} - q_{16,17} \tag{16}$$

$$q_{17} = q_{16,17} - q_{17,0} \tag{17}$$

Equations (1) to (17) in the differential notation take the following form:

$$c_1\dot{T}_1 = c_{dost1} - c_{1,2}(T_1 - T_2) - c_{1,7}(T_1 - T_7) - c_{1,8}(T_1 - T_8) \tag{18}$$

$$c_2\dot{T}_2 = c_{1,2}(T_1 - T_2) + c_{3,2}(T_3) - c_{2,3}(T_2) \tag{19}$$

$$c_3\dot{T}_3 = c_{2,3}(T_2) + c_{5,3}(T_5) - c_{3,2}(T_3) - c_{3,5}(T_3) - c_{3,4}(T_3 - T_4) \tag{20}$$

$$c_4\dot{T}_4 = c_{3,4}(T_3 - T_4) - c_{4,0}(T_4 - T_0) \tag{21}$$

$$c_5\dot{T}_5 = c_{3,5}(T_3) - c_{5,3}(T_3) - c_{5,6}(T_5 - T_6) \tag{22}$$

$$c_6\dot{T}_6 = c_{5,6}(T_5 - T_6) - c_{6,0}(T_6 - T_0) - c_{6,9}(T_6 - T_9) \tag{23}$$

$$c_7\dot{T}_7 = c_{8,7}(T_8 - T_7) + c_{1,7}(T_1 - T_7) - c_{7,0}(T_7 - T_0) \tag{24}$$

$$c_8\dot{T}_8 = c_{1,8}(T_1 - T_8) + \chi c_{9,8}(T_9) + (1-\chi)c_{13,8}(T_{13}) - c_{8,7}(T_8 - T_7) - c_{8,13}(T_8) \tag{25}$$

$$c_9\dot{T}_9 = c_{6,9}(T_6 - T_9) + \chi c_{10,9}(T_{10}) - \chi c_{9,8}(T_9) \tag{26}$$

$$c_{10}\dot{T}_{10} = \chi c_{13,10}(T_{13}) - \chi c_{10,9}(T_{10}) - c_{10,11}(T_{10} - T_{11}) \tag{27}$$

$$c_{11}\dot{T}_{11} = c_{10,11}(T_{10} - T_{11}) - c_{11,12}(T_{11} - T_{12}) \tag{28}$$

$$c_{12}\dot{T}_{12} = c_{11,12}(T_{11} - T_{12}) + c_{0,12}(T_0) - c_{12,0}(T_{12}) \tag{29}$$

$$c_{13}\dot{T}_{13} = c_{14,13}(T_{14} - T_{13}) + c_{8,13}(T_8) - \chi c_{13,10}(T_{13}) - (1-\chi)c_{13,8}(T_{13}) \tag{30}$$

$$c_{14}\dot{T}_{14} = c_{15,14}(T_{15} - T_{14}) - c_{14,13}(T_{14} - T_{13}) - c_{14,0}(T_{14} - T_0) \tag{31}$$

$$c_{15}\dot{T}_{15} = c_{16,15}(T_{16}) - c_{15,16}(T_{15}) - c_{15,14}(T_{15} - T_{14}) \tag{32}$$

$$c_{16}\dot{T}_{16} = c_{dost2} + c_{15,16}(T_{15}) - c_{16,15}(T_{16}) - c_{16,17}(T_{16} - T_{17}) \tag{33}$$

$$c_{17}\dot{T}_{17} = c_{16,17}(T_{16} - T_{17}) - c_{17,0}(T_{17} - T_0) \tag{34}$$

The values of c_i and c_{ij} factors were estimated on the basis of technical documentation of individual elements of the powertrain. The c_i

values describe the unit thermal capacities of the distinguished elements and equal the product of the mass of the element [kg] and its specific heat [kJ/kg·K]. The c_{ij} values describe the heat transfer conditions on the surface of the mentioned element and are equal to the product of the heat transfer surface of the element [m^2] and the heat transfer coefficient on the surface [kJ/m^2·K] (see Table 1).

The model of heating the engine itself without a retarder has been verified experimentally on the engine dynamometer in the Laboratory of Combustion Engines of the Wroclaw University of Technology and Science (Fig. 5). The results obtained from the measurement of the selected parameters describing the operation of the cooling system were used for determining the threshold conditions in the simulation model. Matlab-Simulink package was used for simulation tests (Fig. 6).

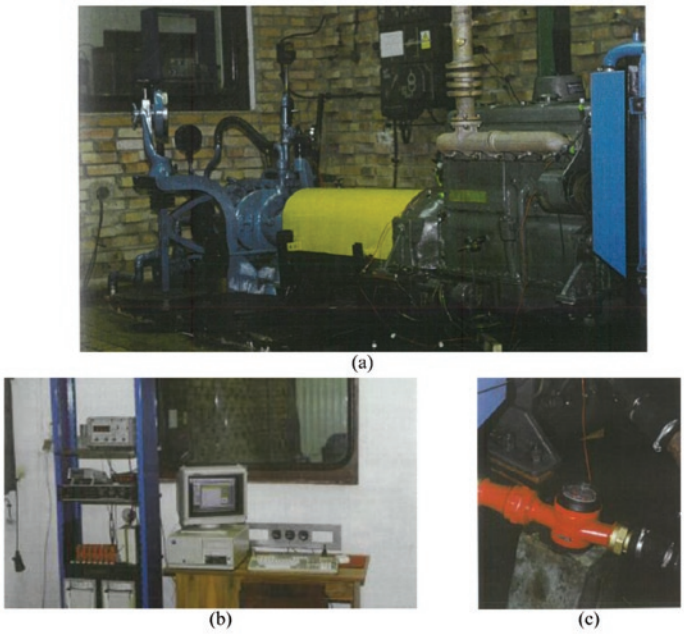

Fig. 5. Pictures of the test stand: (a) view of the 6C107 engine on the engine dynamometer of the Wroclaw University of Technology and Science, (b) computerized test bench on a dynamometer, with a temperature measurement module, (c) view of the engine block coolant flow meter

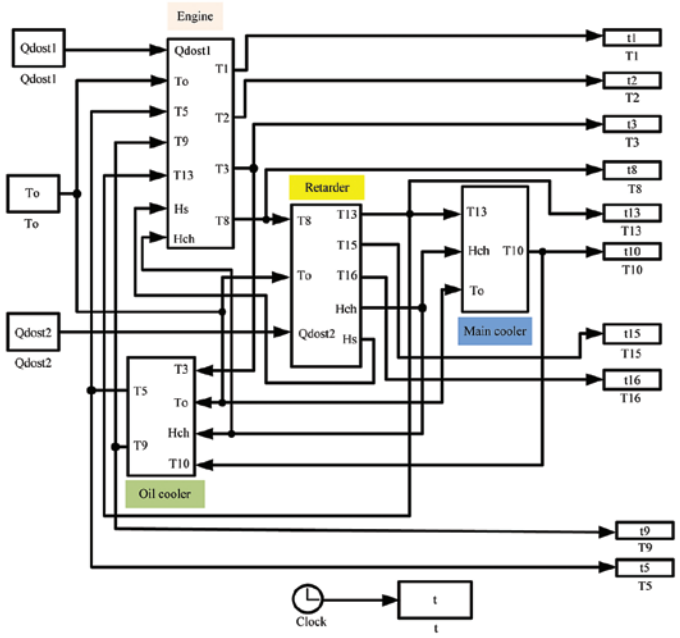

Fig. 6. Matlab-Simulink model

4. Results of simulation tests

Simulation tests were preceded by the development of a test plan. All components of the powertrain, i.e. temperatures from T_1 to T_{16}, distinguished in the temperature model, according to the legend to Fig. 6. A series of tests was carried out taking into account different ambient temperatures, heat exchange surfaces of the radiator, increasing the thermal capacity of the system. The tests used a cooling liquid based on:

a) water-filled engine cooling system,
b) glycol fluid-filled cooling system.

The continuous line indicates temperature fluctuations for the analysed subsystems – T_3, T_8 and T_{16}. The dotted line indicates threshold values in the analysed subsystems.

4.1. Simulation tests of a cooling system at different ambient temperatures

The cooling system tests were carried out at ambient temperatures (T_{ot}) in the range of 253K to 313K every 10K steps. Examples of results are shown in Fig. 7 and Fig. 8. According to them, the system can operate safely in the ambient temperature range up to T_{ot} = 306K (33ºC) (the highest ambient temperatures in Poland reach 313K (40ºC). The improvement of the situation can be achieved by enlarging e.g. the cooler of the engine block coolant.

4.2. Simulation tests of the cooling system for the case of an increase in the heat exchange area of the main cooler

The tests were carried out for three variants of cooler sizes: increased by 10%, by 30% and by 50%, at ambient temperature T_{ot} = 313K (40ºC). The results are presented in Fig. 9.

As can be seen from the presented results, in a glycol-filled system, the use of a cooler with capacity increased by 50% effectively protects all media against exceeding the permissible temperatures, especially the temperature of oil in the retarder. The use of a 50% larger main cooler led to a reduction in oil temperature of about 12K. However, this is not an optimal solution. It is worth investigating the impact that increasing the capacity of the pump in the main cooling system can have on overall capacity.

4.3. Simulation tests of the vehicle cooling system for the case of the cooler increased by 50% and increased coolant flow

The studies were carried out, as in previous cases, for water and glycol at increased flows by 50% and by 100% at ambient temperature T_{ot} = 313K (40ºC). The results are shown in Fig. 10.

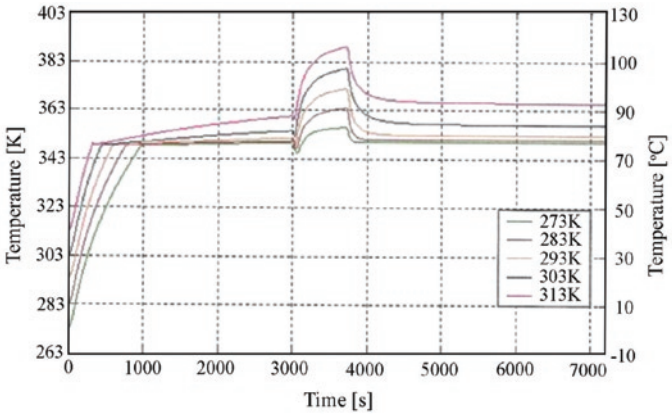

Fig. 7. Trend of cooling liquid temperature changes in engine block at different ambient temperatures (experiment)

Table 1. List of coefficients describing the engine thermal state

No.	A	B	C	D
1	c_i [J/K]	$c_{i,j}$ [W/K]	$c_{i,0}$ [J/K]	other parameters
2	c_1 = 87990	$c_{1,2}$ = 16	$c_{4,0}$ = 1.2	T_0 = 293.15 [K]
3	c_2 = 11750	$c_{1,7}$ = 200	$c_{6,0}$ = 10	q_{dost1} = 29500 [W]
4	c_3 = 1796	$c_{1,8}$ = 998	$c_{7,0}$ = 60	q_{dost2} = 91263 [W]
5	c_4 = 5560	$c_{2,3}$ = 20	$c_{12,0}$ = 13000	T_p = 348 [K]
6	c_5 = 6080	$c_{3,4}$ = 097	$c_{14,0}$ = 12.5	T_k = 358 [K]
7	c_6 = 1800	$c_{3,5}$ = 190	$c_{17,0}$ = 50	-
8	c_7 = 448148	$c_{5,6}$ = 72	-	-
9	c_8 = 20000	$c_{6,9}$ = 100	-	-
10	c_9 = 20950	$c_{8,7}$ = 236	-	-
11	c_{10} = 41900	$c_{9,8}$ = 5866	-	-
12	c_{11} = 19250	$c_{9,10}$ = 5866	-	-
13	c_{12} = 91	$c_{10,11}$ = 955.6	-	-
14	c_{13} = 20960	$c_{11,12}$ = 1240	-	-
15	c_{14} = 4500	$c_{13,18}$ = 5866	-	-
16	c_{15} = 6840	$c_{13,10}$ = 5866	-	-
17	c_{16} = 3040	$c_{14,13}$ = 583	-	-
18	c_{17} = 24750	$c_{15,14}$ = 456	-	-
19	-	$c_{16,15}$ = 5866	-	-
20	-	$c_{16,17}$ = 847	-	-

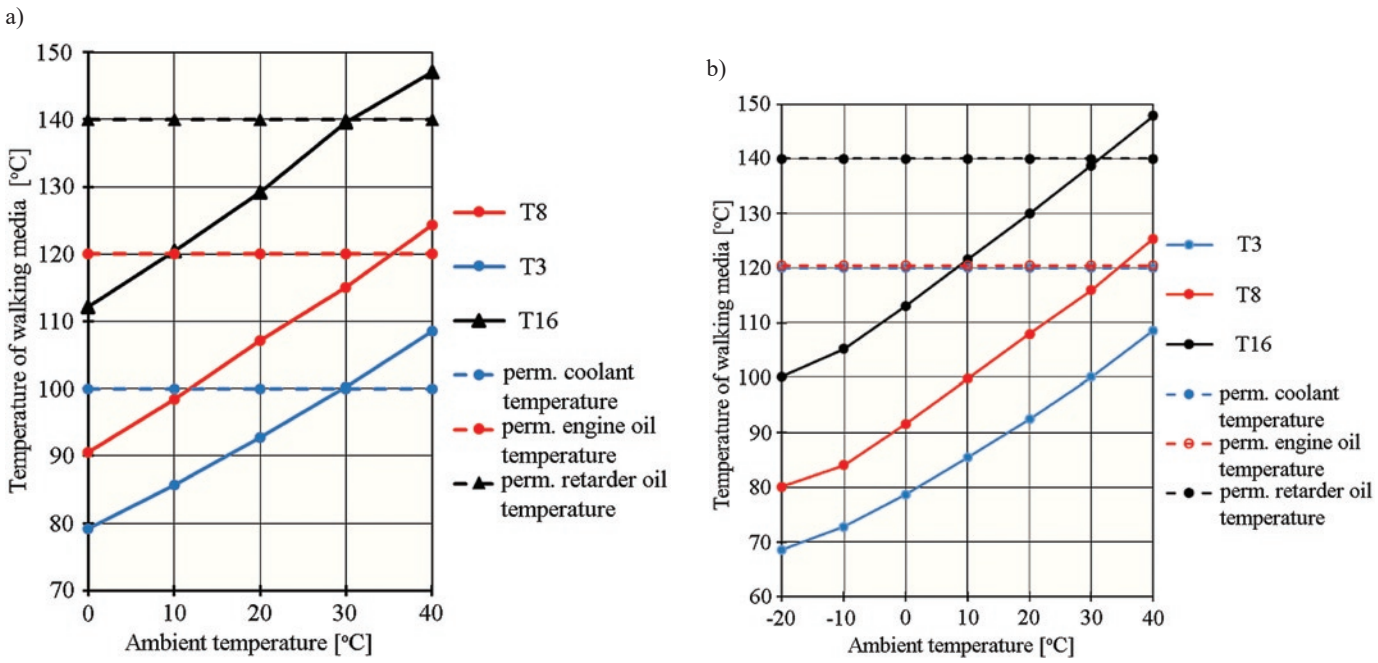

Fig. 8. Temperature of cooling media T_8, T_3, T_{16} versus ambient temperature T_{ot} (experiment): (a) for water, (b) for glycol

Research results show that an effective solution to the problem of temperature reduction in the retarder cooling system can be to increase the pump capacity by 50% or even only by 25% [15, 16].

4.4. Simulation tests of the vehicle's cooling system when an additional coolant tank is used to increase the thermal capacity of the system

The tests were carried out for tanks with a capacity of 20 and 40 dm^3 at an ambient temperature of T_{ot} = 313K (40ºC). The tank was located in the so-called large cooling circuit between the retarder cooler and the main engine cooler. It was assumed that the cooling system is filled with water. The results are shown in Fig. 11.

Equipping the cooling system with an additional coolant tank with a capacity of up to 40 dm^3 causes a slight decrease in system temperature. This solution is ineffective.

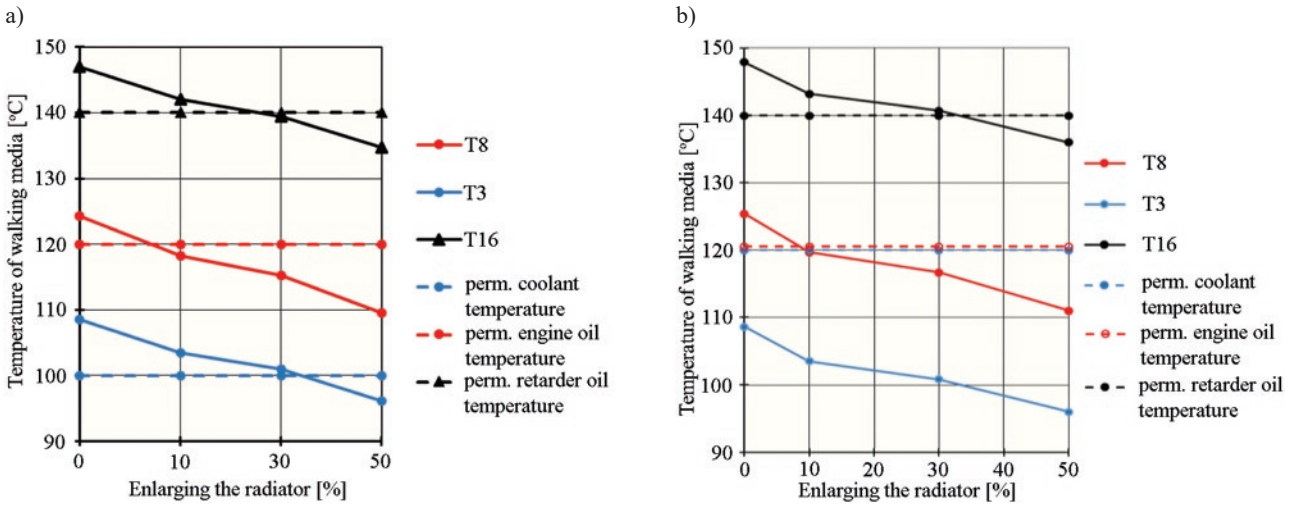

Fig. 9. Temperature of cooling media T_8, T_3, T_{16} versus the size of the radiator T_{ot} (simulation): (a) for water, (b) for glycol

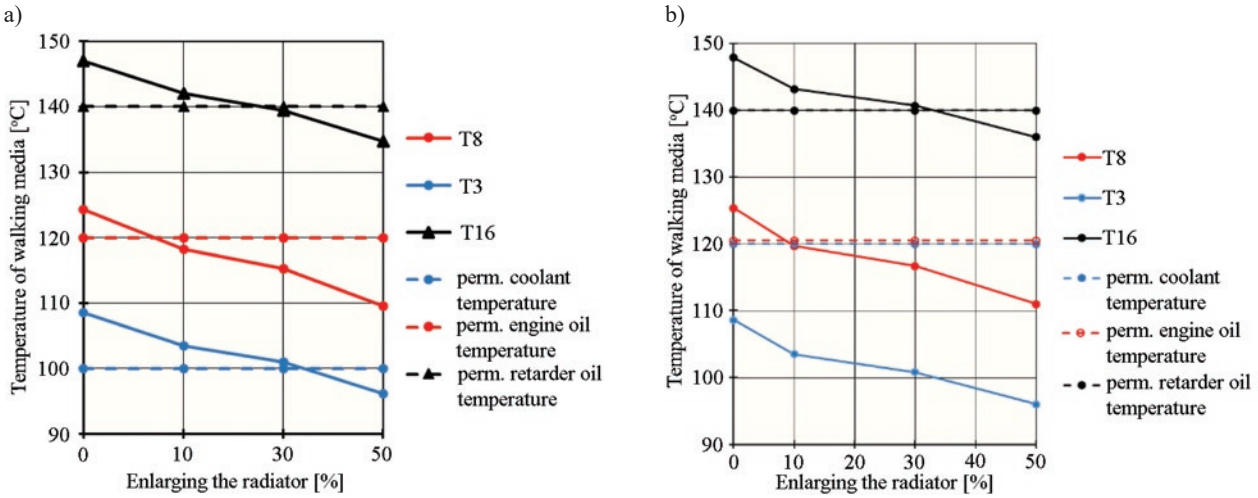

Fig. 10. Temperature of cooling media T_8, T_3, T_{16} versus coolant flow T_{ot} (simulation): (a) for water, (b) for glycol

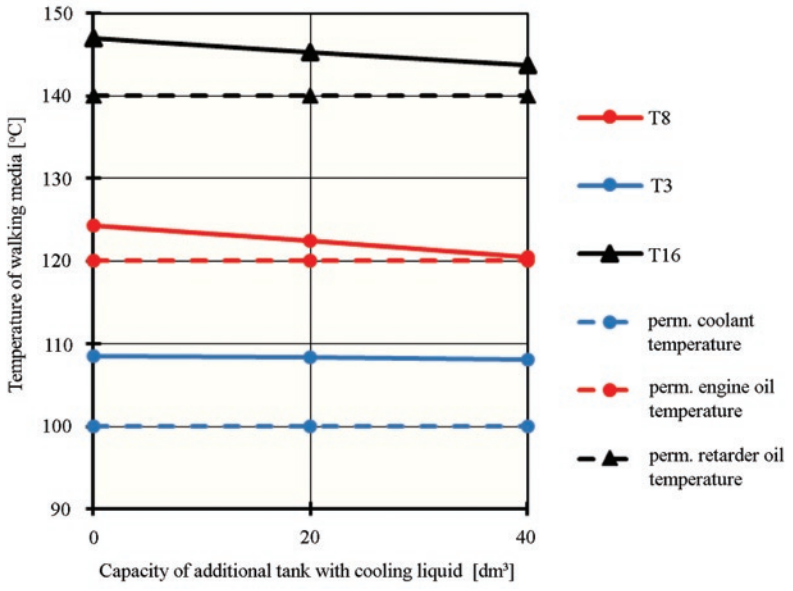

Fig. 11. The dependence of cooling media temperatures on the size of the additional coolant tank (simulation)

5. Conclusion

The aim of the study was to analyze the dynamics of heat exchange in a vehicle equipped with a hydraulic retarder. This device emits large energy flows into the cooling system of the braked vehicle. Therefore, the cooling system should take into account the retarder operation. The requirements in this respect are defined by the relevant EC regulations. On the basis of the analysis of the cooling system structure, a structural and computational model was built. The model of the cooling system is based on a set of 17 balance equations which, according to Newton's principle, were transformed into a set of 17 differential equations describing temperature changes of the distinguished elements versus time. The Matlab-Simulink package was used to solve the equation system. In the study, analyses of the influence of working conditions and constructional conditions on the behaviour of the system in the assumed scenario of its operation were carried out. The results of the work allowed to indicate the direction in which the design of the cooling system of the drive unit should be upgraded so that it could perform its function even in the most difficult working conditions.

References

1. Abe K, Kondoh T, Fukumura K, Kojima M. Three-dimensional simulation of the flow in a torque converter. SAE 1991, https://doi.org/10.4271/910800.
2. Albertz D, Dappen S, Henneberger G. Calculation of the 3D nonlinear eddy current field in moving conductors and its application to braking systems. IEEE Transactions on Magnetics 1996; 32(3): 768-771, https://doi.org/10.1109/20.497353.
3. Baranowski P, Damaziak K, Malachowski J. Brake system studies using numerical methods. Eksploatacja i Niezawodnosc - Maintenance and Reliability 2013; 15(4): 337-341.
4. Baranowski P, Damaziak K, Malachowski J, Mazurkiewicz L, Kastek M, Polakowski H, Piatkowski T. Experimental and numerical tests of thermomechanical processes occurring on brake pad lining surface. Surface Effects and Contact Mechanics 2011; 10: 15-24, https://doi.org/10.2495/SECM110021.
5. Christoffersen S, Wallingford J, Greenlees B. Heavy truck engine retarders. Testing and theory. SAE 2011, https://doi.org/10.4271/2011-01-0280.
6. Dong Y, Korivi V, Attibele P, Yuan Y. Torque converter CFD engineering part I: Torque ratio and K factor improvement through stator modifications. SAE 2002, https://doi.org/10.4271/2002-01-0883.
7. ECE Regulation No. 13, Uniform provisions concerning the approval of vehicles of categories M, N and O with regard to braking.
8. Gohring E, Glasner EC, Povel R. Engine braking systems and retarders - an overview from European standpoint. SAE 1992, https://doi.org/10.4271/922451.
9. Habib G. The present status of electro-magnetic retarders in commercial vehicles. SAE 1992, https://doi.org/10.4271/922450.
10. Haiss G. Demand criteria on retarders. SAE 1992; https://doi.org/10.4271/922453.
11. Heisler H. Advanced Vehicle Technology. Second Edition. Butterworth-Heinemann: Elsevier Ltd., 2002.
12. Jeyakumar S, Sasikumar M. Computational fluid dynamics simulation of hydraulic torque converter for performance characteristics prediction. International Journal of Scientific Research in Science, Engineering and Technology 2017; 3(6): 402-408.
13. Jia Y H. Dynamic simulation research of hydrodynamic retarder in brake process. Proceedings 2011 International Conference on Transportation, Mechanical, and Electrical Engineering (TMEE) 2011: 1193-1196.
14. Kazmierczak A, Krakowian K, Wrobel. Doppler Laser Vibrometry in combustion engine's diagnosis. Przeglad Elektroniczny 2010; 86(10): 147-149.
15. Kern J, Ambros P. Concepts for a controlled optimized vehicle engine cooling system. SAE 1997, https://doi.org/10.4271/971816.
16. Kesy A, Kadziela A. Construction optimization of hydrodynamic torque converter with application of genetic algorithm. Archives of Civil and Mechanical Engineering 2011; 11(4): 905-920, https://doi.org/10.1016/S1644-9665(12)60086-7.
17. Kwasniowski S, Sroka Z. Modeling dynamics of heat exchange in cooling, heating and air conditioning systems of vehicles and working machines. Wroclaw: Series report SPR No. 075/97, Wroclaw University of Technology, 1998.
18. Lei Y, Song P, Zheng H, Fu Y, Li X, Song B. Application of fuzzy logic in constant speed control of hydraulic retarder. Advances in Mechanical Engineering 2017; 9(2): 1-11, https://doi.org/10.1177/1687814017690956.
19. Li J, Tan G, Ji Y, Zhou Y, Liu Z, Xu Y. Design and simulation analysis for an integrated energy-recuperation retarder. SAE Technical Paper 2016, https://doi.org/10.4271/2016-01-0458.
20. Li R, Yang J, Zhang W. Simulation Study of the Vehicle Hydraulic Retarder, International Journal of Control and Automation 2015; 8(2): 263-280, https://doi.org/10.14257/ijca.2015.8.2.26.
21. Liu C Y, Jiang K J, Zhang Y. Design and use of an eddy current retarder in an automobile. International Journal of Automotive Technology 2011; 12(4): 611-616, https://doi.org/10.1007/s12239-011-0071-3.
22. Marechal Y, Meunier G. Computation of 2D and 3D eddy currents in moving conductors of electromagnetic retarders. IEEE Transactions on Magnetics1990; 26(5): 2382-2384, https://doi.org/10.1109/20.104738.
23. Mu H, Yan Q, Wei W. Study on influence of inlet and outlet flow rates on oil pressures and braking torque in a hydrodynamic retarder. International Journal of Numerical Methods for Heat & Fluid Flow 2017; 27(11): 2544-2564, https://doi.org/10.1108/HFF-10-2016-0428.
24. Pandey S N, Khaliq A, Zaka M Z, Saleem M S, Afzal M. Retarder used as braking system in heavy vehicles - a review. International Journal Mechanical Engineering and Robotic Research 2015; 4(2): 86-90.
25. Peng Z. A Study into the technology of development of hydraulic. Xi'an: Chang'an University, 2008.
26. Pernestål A, Nyberg M, Warnquist, H. Modeling and inference for troubleshooting with interventions applied to a heavy truck auxiliary braking system. Engineering Applications of Artificial Intelligence 2012; 25(4): 705-719, https://doi.org/10.1016/j.engappai.2011.02.018.
27. Song B, Lv J, Liu Y, Kong F. The simulation and analysis on engine and hydraulic retarder continual braking performance of the tracked vehicle on long downhill. Proceedings 9th International Conference on Electronic Measurement & Instruments 2009: 3-928-3-931, https://doi.org/10.1109/ICEMI.2009.5274169.
28. Sarkar S, Rathod P P. Review paper on thermal analysis of ventilated disc brake by varying design parameters. International Journal of Engineering Research & Technology 2013; 2(12): 1077-1081.
29. Tan G, Guo X, Yang T. Simulation based heavy truck driveline components thermal analysis system. The 9th International Conference on, Electronic Measurement & Instruments, ICEMI'2009: 4-675-4-680, https://doi.org/10.1109/ICEMI.2009.5274676.
30. Tan G, Guo X. The modeling and performance analysis of the retarder thermal management system. SAE 2012, https://doi.org/10.4271/2012-01-1929.
31. Wambsganss M W. Thermal management in heavy vehicles: a review identifying issues and research requirements. Argonne National Lab., IL (US), No. ANL/ET/CP-98208, 1999.
32. Wangand G, Shan S. Review of meta modeling techniques in support of engineering design optimization. Journal of Mechanical Design, Transactions of the ASME 2007; 129(4): 370-380, https://doi.org/10.1115/1.2429697.
33. Wrzecioniarz P, Kwasniowski S, Jamroziak K. Criterion for choosing the power unit cooling system of evacuation tractor. Czasopismo Techniczne Mechanika 1998; 95(5-M): 83-93.
34. Wrzecioniarz P, Kwasniowski S, Jamroziak K. The concept of the cooling system for the road tractor unit. Pojazdy samochodowe: problemy

rozwoju jakości, VI Międzynarodowa Konferencja Naukowo-Techniczna "Autoprogres'98" 1998; T.2: 127-134.
35. Xin Q. Diesel engine system design. New Delhi: Woodhead Publishing, 2011, https://doi.org/10.1533/9780857090836.
36. Yang J, Yi F, Wang J. Model-based adaptive control of eddy current retarder. Proceeding of the 30th Chinese Control And Decision Conference (2018 CCDC) 2018; 1889-1891, https://doi.org/10.1109/CCDC.2018.8407434.
37. Zheng H, Lei Y, Song P. Design of a filling ratio observer for ahydraulic retarder: An analysis ofvehicle thermal management and dynamic braking system. Advances in Mechanical Engineering 2016; 8(10): 1-8, https://doi.org/10.1177/1687814016674098.
38. Zheng H, Lei Y, Song P. Hydraulic retarders for heavy vehicles: Analysis of fluid mechanics and computational fluid dynamics on braking torque and temperature rise. International Journal of Automotive Technology 2017; 18(3): 387-396, https://doi.org/10.1007/s12239-017-0039-z.
39. Zhou L, Tan G, Guo X, Chen M, Ji K, Li Z. Yang Z. Study of energy recovery system based on organic rankine cycle for hydraulic retarder. SAE 2016, https://doi.org/10.4271/2016-01-0239.

Krzysztof JAMROZIAK
Stanislaw KWASNIOWSKI
Mariusz KOSOBUDZKI
Pawel ZAJAC
Faculty of Mechanical Engineering,
Wroclaw University of Science and Technology
ul. Wyb. Wyspianskiego 27, 50-370 Wroclaw, Poland

E-mails: krzysztof.jamroziak@pwr.edu.pl, stanislaw.kwasniowski@pwr.edu.pl, mariusz.kosobudzki@pwr.edu.pl, pawel.zajac@pwr.edu.pl